Understanding KOtBu in Atomic Layer Deposition - *in situ* Mechanistic Studies of the KNbO₃ Process

Journal:	*Dalton Transactions*
Manuscript ID	DT-ART-07-2020-002324.R1
Article Type:	Paper
Date Submitted by the Author:	28-Jul-2020
Complete List of Authors:	Sønsteby, Henrik; University of Oslo, Chemistry Killi, Veronica; University of Oslo, Chemistry Storaas, Thomas; University of Oslo, Chemistry Choudhury, Devika; Argonne National Laboratory, Energy Systems Division Elam, Jeffrey; Argonne National Laboratory, Energy Systems Division Fjellvåg, Helmer; University of Oslo, Chemistry Nilsen, Ola; University of Oslo, Department of Chemistry

ARTICLE

Understanding KOᵗBu in Atomic Layer Deposition - *in situ* Mechanistic Studies of the KNbO₃ Process

Henrik H. Sønsteby[a,b]*, Veronica A.-L. K. Killi[a], Thomas A. Storaas[a], Devika Choudhury[b], Jeffrey W. Elam[b,c], Helmer Fjellvåg[a] and Ola Nilsen[a]*

Functional coatings based on alkali metals become increasingly attractive in the current shift towards sustainable technologies. While lithium based compounds have a natural impact in batteries, the other alkali metal compounds are important as replacements for toxic materials in a range of electronic devices. This is especially true for potassium, being a major component in *e.g.* $K_xNa_{1-x}NbO_3$ (KNN) and $KTa_xNb_{1-x}O_3$ (KTN), with hope to replace $Pb(Zr_xTi_{1-x})O_3$ (PZT) in piezo-/ferroelectric and electrooptic devices. Using ALD facilitates functional conformal coatings at deposition temperatures far below what is reported by other techniques and with excellent compositional control. The ALD growth of potassium containing films using KOᵗBu has, however, been unpredictable. Untraditional response to pulsed composition and precursor dose, severe reproducibility issues and very high growth per cycle are some of the puzzling features of these processes. In this article, we shed light on the growth behavior of KOᵗBu in ALD using *in situ* quartz crystal microbalance and Fourier transform infrared spectroscopy. We study the precursor's behavior in the technologically interesting KNbO₃-process, showing how the potassium precursor strongly affects growth of other cation precursors. We show that the strong hygroscopic nature of the intermediary potassium species has far-reaching implications throughout growth. This serves not only to enhance the understanding of alkali metal containing growth in ALD, but also to provide means to control growth of novel sustainable technological materials.

Introduction

Alkali metal containing compounds play a major role in the transition from lead based dielectrics. The most applicable example is LiNbO₃ as dielectric and the recent development of lithium based processes for ALD.[1,2] The unproportioned interest for lithium is, however, mainly due to the development in lithium ion batteries. While lithium based processes were introduced more than 10 years ago, and its growth has been thoroughly investigated using in situ techniques in the following years, development of processes for the other alkali elements lags behind.[3-5] This is somewhat surprising, considering the minute mass and analysis cross section of lithium compared to the other alkaline elements. ALD processes for Na/K and Rb were introduced in 2014 and 2017, respectively.[6,7]

Examples of important alkali containing compounds are sodium in low-cost batteries and thermoelectric sodium cobaltite, and rubidium and cesium as dopants in record-breaking perovskite solar cells.[8-12] More pertinent, however, is the implementation of potassium containing materials as replacements in lead-

containing devices, which are widespread in sensors, actuators, transducers and in emerging non-volatile memory technology. $K_xNa_{1-x}NbO_3$ (KNN) is one of few materials that have the necessary piezoelectric coefficients and tunability to compete with lead-based ferroelectrics.[13] Furthermore, $KTa_xNb_{1-x}O_3$ (KTN) is another para-/ferroelectric material with strong electro-optical behavior, which is highly sought for use in efficient integrated photonics. [14,15]

Many of these applications requires active components in the form of thin films. Traditional techniques for depositing oxides, such as MBE and PLD, come short due to uncontrollable loss of alkali metal at elevated temperatures. ALD is emerging as a facile option for deposition of potassium containing thin films, and have recently been used to deposit both KNN and KTN.[16-18] Films are deposited at low temperatures, and require only moderate post-deposition annealing to obtain highly oriented crystalline films on a range of substrates. In both of these studies, in addition to the inaugural K_xAlO_y work, potassium *tert*-butoxide (KOᵗBu) is used as the potassium source. This precursor type is well-known from lithium ALD-processes; known to enable clean chemistry for deposition of complex lithium containing compounds.[3] KOᵗBu has a favorable vapor pressure, with one clean sublimation leaving very little residual mass.[6] It is hygroscopic and degrades fast in air, but is stable if treated under inert conditions.

a. Department of Chemistry, University of Oslo, Blindern, 0315 Oslo, Norway
b. Argonne National Laboratory, Argonne, Illinois 60439, USA
c. Advanced Materials for Energy-Water Systems (AMEWS) Energy Frontier Research Center (EFRC), Lemont, IL 60439, USA
* henrik.sonsteby@kjemi.uio.no, ola.nilsen@kjemi.uio.no

From the reported potassium processes, it is clear that KO^{t}Bu behaves quite different than its lithium- and sodium counterparts. Potassium processes leads to very high K-incorporation for low pulsed ratios, high growth per cycle (GPC) and are difficult to reproduce due to memory- and reservoir effects.[6,16-18] While LiO^{t}Bu and NaO^{t}Bu both predominantly take hexamer form in gas phase, KO^{t}Bu is a tetrameric cubane-like structure in the gas phase (Figure 1).[19] To enable controlled deposition of a wide range of potassium containing thin films with ALD, it is necessary to understand the growth at a finer level.

In this work, we use *in situ* quartz crystal microbalance (QCM) and Fourier Transform Infrared Spectroscopy (FT-IR) to shed light on the mechanisms that govern ALD growth of potassium containing films. QCM reveals information on intermediary and net mass variation on the surface as the process runs. FT-IR enables discussion on the chemical nature of the surface species that are found during deposition. Together, the two techniques enable a stringent discussion on the chemistry of an ALD process.

We chose the complex K-Nb-O process over the K-O(H) process due to inherent challenges with reservoir effects of the latter process, and also to provide information on a more technologically interesting material. This also enables a deeper understanding on how the use of KO^{t}Bu affects growth of other precursors in a complex process. We find that the chemistry involved is surprisingly clean and ALD-type of nature, but that uncommon reactions alter the surface chemistry in a way that must be considered when developing new processes for potassium-containing thin films. The large K-incorporation is found to be a result of the tetrameric shape of the precursor molecule, and the high growth rates can be explained by a significant water uptake as a result of the hygroscopic nature of intermediary species.
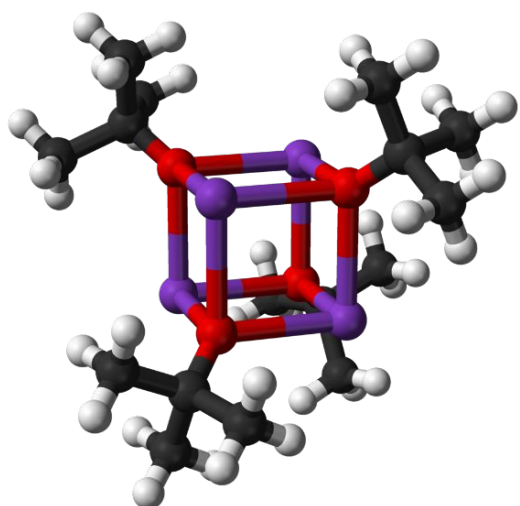

Figure 1: Tetramer of KO^{t}Bu, found to be the predominant gas phase species.

These findings reveal important information on the growth of potassium containing thin films by ALD. Furthermore, given that RbO^{t}Bu and CsO^{t}Bu take the same structure as KO^{t}Bu, these results also have implications for the understanding of Rb- and Cs-containing ALD. We believe this extended understanding of potassium ALD will aid the transition to sustainable materials in future technology.

Experimental

Thin films for compositional and QCM analysis were deposited in an F-120 Sat ALD reactor (ASM Microchemistry). The deposition temperature was maintained at 250 °C under an operating pressure of 2.4 mbar, maintained by a 300 cm^3 min^{-1} primary flow rate of N$_2$. Nitrogen was supplied from gas cylinders (Praxair, 99.999 %) and run through a Mykrolis purifier for removal of any oxygen or water contamination.

KO^{t}Bu (Aldrich, 97 %) and Nb(OEt)$_5$ (Sigma-Aldrich, 99 %) were used as cation sources, supplied from open boats inside the reactor at 150 and 80 °C, respectively. De-ionized H$_2$O was used as oxygen source, supplied from a bubbler outside the reactor kept at room temperature. 3 x 3 cm^2 Si (100) substrates were used for compositional analysis.

In situ QCM was carried out using two 6 MHz AT-cut quartz crystals (Inficon, Ø = 1.4 cm), mounted approximately 5 cm apart in a homemade holder. An EON-LT (Colnatec) was used to collect frequency changes in the crystals. The relationship between frequency and mass change was established by calibrating towards growth of Nb$_2$O$_5$, with known GPC and density, as explained under *Results and Discussion - Calibration*. The reactor temperature was stabilized before performing the QCM experiment to ensure reliable frequency-mass response.

In situ FT-IR was carried out using a Nicolet 6700 FTIR Spectrometer (Thermo Scientific) mounted on a separate home-built ALD reactor (Argonne National Laboratory). The spectrometer was operated in transmission mode, utilizing gate valves that close upon pulsing and open during IR exposure to avoid deposition on the IR-transparent KBr windows. ZrO$_2$ nanopowder (Aldrich, < 100 nm) loaded on a fine stainless steel grid (mask size 200 µm) was used as substrate, due to its high IR-transparency in the 800 − 4000 cm^{-1} frequency range. The grid was mounted onto a heating stage and heated to 250 °C throughout the deposition. The reactor chamber walls were maintained at 250 °C, and N$_2$ (99.9999 %, Airgas) was used as purging gas, supplied form gas bottles. Precursors were kept in external bubblers connected to the reactor with heated stainless steel lines. Precursor temperatures were kept the same for composition and QCM-experiments.

The chemical composition for KNbO$_3$ films was analyzed using an Axios Max Minerals x-ray fluorescence (XRF) system (Panalytical), equipped with a 4 kW Rh-tube. The system runs using Omnian and Stratos options for standardless measurement of thin films.

Routine measurements of thickness were carried out on an alpha-SE spectroscopic ellipsometer (J.A. Woollam) in the $390 - 900$ nm wavelength range. We successfully employed a Cauchy function to model the collected data. X-ray reflectivity (XRR) was used as a complementary method to determine thickness and densities of Nb_2O_5 calibration samples.

Results and Discussion

Calibration – Nb_2O_5

The frequency response to mass variation for the QCM crystal used throughout the study was calibrated by measuring its response of pure Nb_2O_5 growth, using $Nb(OEt)_5$ and water as precursors. The calibration was carried out under steady-state conditions, after 100 Nb_2O_5 cycles to prime the surface. This process is highly reproducible and stable, with a GPC of 0.38 Å cyc^{-1} and a density for as deposited amorphous films (at 250 °C) of 4.32 ± 0.05 g cm^{-3}, as measured by XRR. [20] The mass gain per unit area for a $Nb(OEt)_5$ + H_2O cycle can be calculated by:

$$\Delta m = \text{ GPC} \cdot \rho_{Nb_2O_5} = 16 \text{ ng cm}^{-1} \text{ cyc}^{-1} \qquad \text{Eq. 1}$$

where $\rho_{Nb_2O_5}$ is the measured density of Nb_2O_5 thin films and GPC is the averaged growth per cycle for $Nb(OEt)_5$ + H_2O in the steady growth regime. It is well known that niobium(V)ethoxide is a dimer in gas phase (Figure 2).[21] However, for simplicity (and since the net mass variation will be the same over a given area), we treat the chemical reactions taking place on the surface by the classic view with niobium(V)ethoxide monomers. A representative cycle for $Nb(OEt)_5$ + H_2O as measured by QCM is shown in Figure 3. The mass gain is large as the heavy niobium(V)ethoxide reacts with the surface (green), with some mass decrease due to desorption upon the subsequent purge (orange). Water from the succeeding pulse reacts with remaining ethoxide ligands creating ethanol, leaving the surface and further reducing the mass.

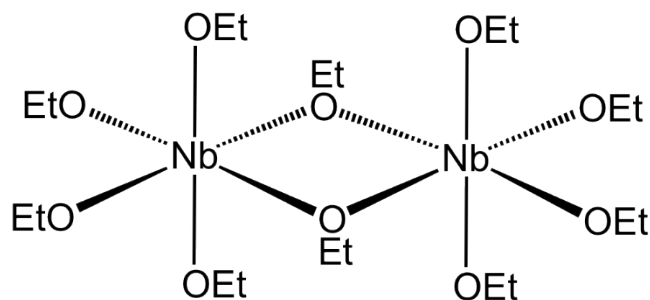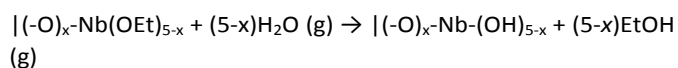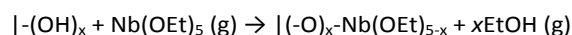The reactions taking place are hypothesized to be:

$|\text{-(OH)}_x + \text{Nb(OEt)}_5 \text{ (g)} \rightarrow |\text{(-O)}_x\text{-Nb(OEt)}_{5-x} + x\text{EtOH (g)}$

$|\text{(-O)}_x\text{-Nb(OEt)}_{5-x} + (5-x)\text{H}_2\text{O (g)} \rightarrow |\text{(-O)}_x\text{-Nb-(OH)}_{5-x} + (5-x)\text{EtOH (g)}$

Figure 3: One representative cycle of $Nb(OEt)_5$ + H_2O as measured by QCM. Colored fields indicate $Nb(OEt)_5$ pulse (green), purge (orange), water pulse (blue) and purge (orange), respectively.

For the $Nb(OEt)_5$ and H_2O pulses, respectively. Ethanol is the only by-product formed as previously shown by Ritala *et al.*[22] Using the measured mass gain as measured from QCM, the amount of leaving ethoxy groups during the two separate pulses was found to be 3.7 for the $Nb(OEt)_5$ and 1.3 for the H_2O pulse, i.e. $x = 3.7$.

This is better understood when viewing niobium(V)ethoxide as a dimer, reacting horizontally so that both niobium atoms are coordinated to the surface, with the two vertically aligned ethoxide groups (and possibly one of the bridging ethoxide groups) persisting until the water pulse.

The persisting ethoxide groups can be observed using *in situ* FT-IR. Figure 4 shows saturation of $Nb(OEt)_5$ (a) and water (b) during their respective pulses, on –OH terminated and $Nb(OEt)_5$ terminated surfaces, respectively. Signals in the $1200 - 1000$ cm^{-1} range can be attributed to asymmetric C-O- and C-C stretch modes, with some variability depending on the coordination to Nb. It is evident that ethoxy groups are present on the surface upon saturation of $Nb(OEt)_5$ (Figure 4 a). The persisting ethoxy groups then react with water and are gradually removed until there are no ligands left (Figure 4 b).

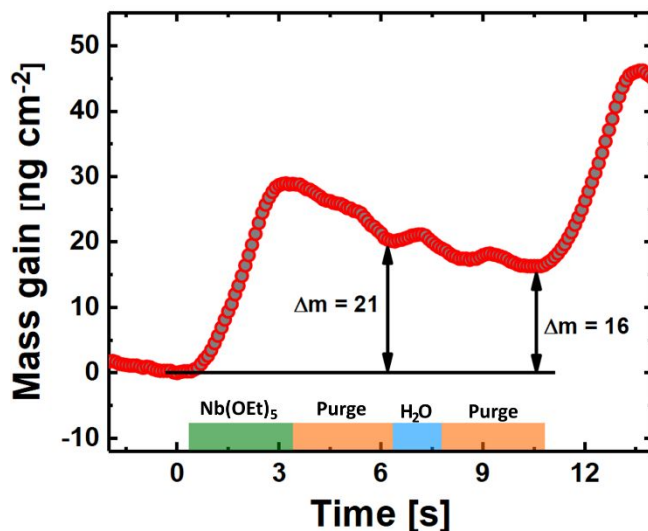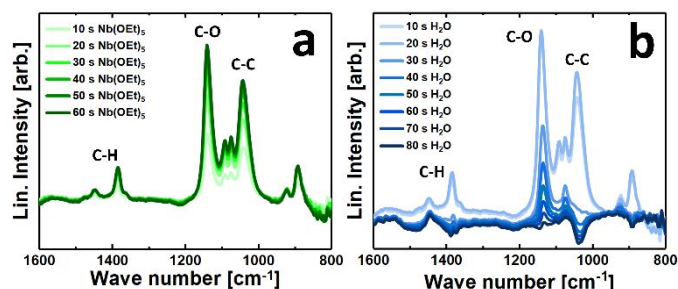Figure 2: Dimer of Nb(OEt)5, found to be the predominant gas phase species.

Figure 4: Saturation for $Nb(OEt)_5$ (a) and H_2O (b), as measured by FT-IR (difference spectra).

Note that the character of the signals from asymmetric C-O and C-C stretches change upon water pulsing. After 30 seconds, the complex shape of the signal has disappeared completely. This suggests that either the monocoordinated Nb-OEt or the bicoordinated Nb-OEt-Nb from the dimeric precursor reacts first with water, leaving only one of these species left on the surface. This does not seem to affect further growth, as no ligands persist after prolonged dosing of water. To emphasize the changes happening on the surface during a full cycle, we present net cycle difference spectra in supporting information (Supporting Figure A).

The KO^{t}Bu pulse

Investigating growth of pure KO$_x$/KOH has proved difficult due to large variations in signature as the mass of deposited material builds up. The growth rapidly becomes uncontrolled, most likely due to the strong hygroscopic nature of the alkali metal oxide and/or hydroxide species. As a result of this, we studied the "pure" KO^{t}Bu + H$_2$O process for a 1:1 pulsing regime of KO^{t}Bu to Nb(OEt)$_5$. In other words, note that this characterization of the KO^{t}Bu + H$_2$O process takes place on a partially –Nb(OH)$_x$ terminated surface. QCM was again employed to investigate the mass gain during the process (Figure 5). Compared to the Nb(OEt)$_5$ pulse, KO^{t}Bu exhibits a massive mass gain, even though K has a much lower atomic mass than Nb (31.2 vs. 92.9 a.u.). This should mean that the amount of K incorporated in each pulse is much larger than what is incorporated for Nb. By combining with previous work on LiO^{t}Bu, a natural hypothesis for the reactions that are taking place is:
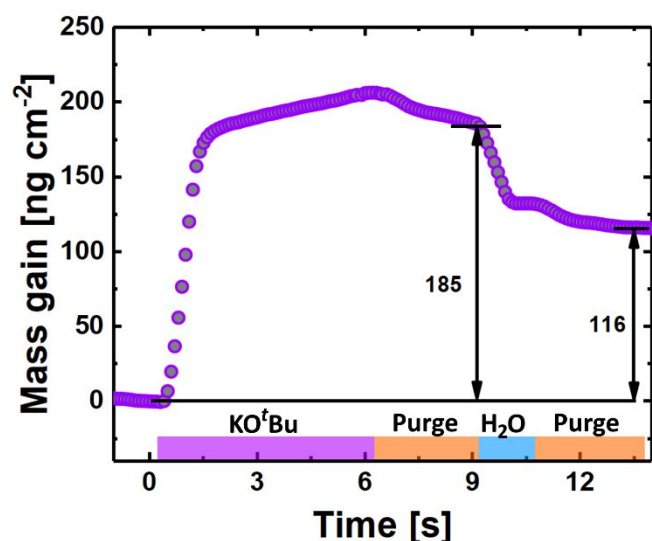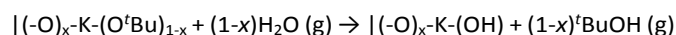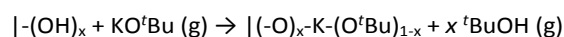
$$|-(OH)_x + KO^tBu\ (g) \rightarrow |(-O)_x-K-(O^tBu)_{1-x} + x\ ^tBuOH\ (g)$$

$$|(-O)_x-K-(O^tBu)_{1-x} + (1-x)H_2O\ (g) \rightarrow |(-O)_x-K-(OH) + (1-x)^tBuOH\ (g)$$

Figure 5: One representative cycle of KO^{t}Bu + H$_2$O as measured by QCM. Colored fields indicate KO^{t}Bu pulse (purple), purge (orange), water pulse (blue) and purge (orange), respectively.

Using the theoretical density for KOH (2.12 g cm^{-3}) and an estimated GPC for KO^{t}Bu + H$_2$O of 1.2 Å cyc^{-1} found by extrapolation of GPCs for varying ratios of KO^{t}Bu:Nb(OEt)$_5$ (Supporting Figure B) this converts to an expected mass gain of 25.4 ng cm^{-1} cyc^{-1}. The actual measured value is close to 4.5 times the theoretical gain.

Once again, it is important to remember that many precursor molecules are not monomers. As previously mentioned, it has been shown that KO^{t}Bu is a tetramer, adopting a cubane-like structure also in gas phase (Figure 1).[19] Even though the net reactions taking place will not be different, this may help in describing the large mass gain that is observed. If the cubane like structure reacts with the surface to release only one of its four *tert*-butoxide ligands as butanol, the net mass increase per adsorbed precursor species would be ~375 a.u. A mass gain of 185 ng cm^{-1} after the KO^{t}Bu pulse and purge would amount to a surface density of such K$_4$(O^{t}Bu)$_3$-species of ~0.3 · 10^{15} cm^{-2}. A mean intraplanar O-O distance of 2.66 Å for Nb$_2$O$_5$ amount to a maximum –OH surface density of ~1.4 · 10^{15} cm^{-2}, meaning that approx. every 5th –OH site has reacted with a potassium *tert*-butoxide tetramer. If we consider the KO^{t}Bu tetramer a circle (with an estimated Ø = 8 Å based on bond-length and bond angle considerations) chemisorbed on an O-site in the –OH-terminated lattice, and then close-pack these circles, each precursor molecule occupies 9 –OH sites (Supporting Figure C). It is however probable, that the tetramers can pack closer, since the *tert*-butoxy ligands do not occupy the full circle area but stick out like arms from the (KO)$_4$ cube. In any case, based on the measured mass gain, it is clear that the full tetramer units must be chemisorbed and that they cover the surface with a very high areal density.

However, if the tetramer adsorbs and deposits four K-atoms per reacted site, the mass drop should have been more dramatic during the water pulse. The ratio between the mass gain after the KO^{t}Bu and the mass drop after the water pulse would be ~2.2 in the theoretical case, while we measure a ratio of ~3.13. However, since there is a mass drop upon purging after the KO^{t}Bu pulse, it is possible that some of the *tert*-butoxide ligands is removed from the surface during the purge. This could either be in the form of decomposing tetramers with butanol as byproduct, or via complete desorption of tetramer species and formation of KOH. Note that there is also a possibility that KO^{t}Bu reacts with a water reservoir in the films, which could explain the large mass gain. This could also help explain the smaller mass drop upon water pulsing.

Based on these observations, we hypothesize that the reaction between KO^{t}Bu and the surface is complex, with several reactions taking place. The governing reaction, however, is believed to be dense chemisorption of full tetramer units of KO^{t}Bu, and then subsequent reaction with water to form a large amount of KOH.

Since the KO^{t}Bu reaction behavior has not been previously studied, we also carried out a quick analysis of the implication

of prolonged dosing and purge (Figure 6). We observe that doubling the duration of the purge after the KO^{t}Bu pulse from 3 to 6 s does not change the net growth, but that the water uptake (and release) is more prominent with increased purge. Note that the experiment with prolonged purge was carried out at a later stage in the experiment, and that the additional water uptake and release could be a result of increased bulk that absorb more water. Furthermore, we observe that doubling the dose of KO^{t}Bu slightly *does* increase the net growth. After an initial rapid mass gain that is similar for 3 and 6 s pulsing, growth slows down but does not seem to completely stop. There are three probable causes for this behavior: Polymerization of KO^{t}Bu (larger polymers than the tetramer is known to exist for other alkali metal *tert*-butoxides), decomposition of the precursor into KOH and butane, or reaction with water stored in a reservoir from previous water exposure.

To identify the governing mechanism for the additional growth, we carried out FT-IR saturation measurements for the KO^{t}Bu and subsequent water pulsing. KO^{t}Bu is found to rapidly saturate in terms of concentration of butoxy groups (Figure 7 a), much faster in fact than what is observed for Nb(OEt)$_5$. On prolonged dosing, the signal originating from asymmetric C-O and C-C stretches does not increase in magnitude. We do observe, however, signals coming from KOH (at ~ 1480 cm^{-1}) during the water pulse. This indicates that further polymerization of KO^{t}Bu is not probable, but that formation of some KOH may take place even on KO^{t}Bu pulsing, either through decomposition or reaction with a water reservoir. This is further backed up by later FT-IR experiments (see figure 16 and surrounding discussion). Note that the FT-IR experiments are carried out with far fewer total cycles than the QCM experiments, and that any bulk water reservoir will probably affect the QCM measurements to a greater extent since the bulk of the film is thicker and may store more water. The reaction with chemisorbed KO^{t}Bu upon pulsing water is equally fast as the saturation of KO^{t}Bu, removing any butoxy ligands and forming KOH (Figure 7 b) as expected.
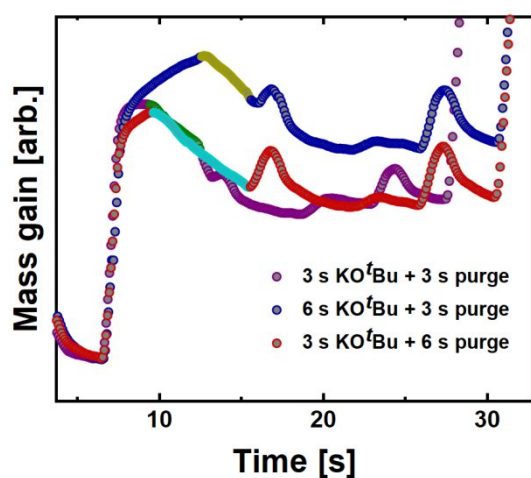

Figure 7: Saturation for KO^{t}Bu (a) and H$_2$O (b), as measured by FT-IR (difference spectra). Note that the surface is terminated by Nb$_2$O$_5$ after 20 cycles of Nb(OEt)$_5$ + H$_2$O prior to the saturation experiment.

A difference FT-IR spectrum after KO^{t}Bu (purple) and H$_2$O (blue) saturation is shown in Supporting Figure D to emphasize the changes happening on the surface during a full cycle. We also studied the growth behavior of subsequent KO^{t}Bu + H$_2$O cycles (with no Nb$_2$O$_5$ cycles in between), to shed light on the uncontrollable growth that is observed under normal film growth (Figure 8). Surprisingly, the process seems to behave relatively stringent. The saturation concentration of butoxy ligands is relatively unchanged, while the KOH feature grows. It is probable that excess surface KOH, with a large amount of
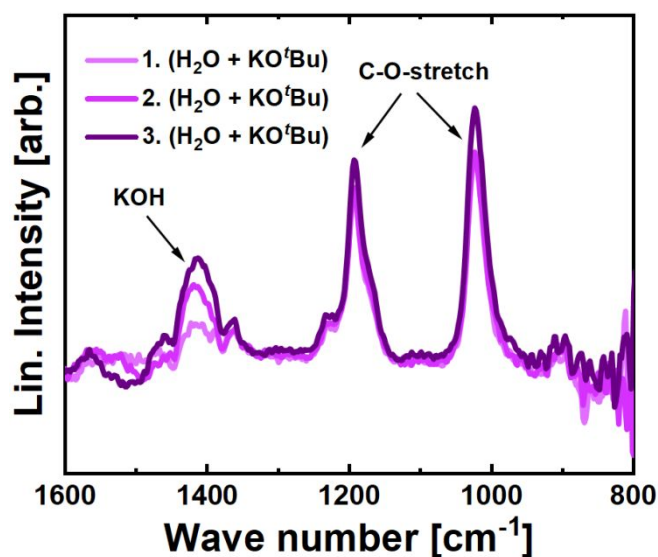
water due to its hygroscopic nature, may interfere with continued growth of KOH and Nb$_2$O$_5$. This may be an explanation to why we observe uncontrolled growth for processes with excess pulsing of KO^{t}Bu, with formation of films that rapidly react with air upon breaking vacuum. As an intermediary conclusion, it is clear that the reaction between KO^{t}Bu and the surface does not exhibit traditional ALD saturation, but a more complex behavior. This is most likely an effect of a bulk water reservoir that leads to excessive growth of KOH upon KO^{t}Bu pulsing, or due to decomposing KO^{t}Bu upon reaction with KOH.

Figure 6: Three different timing regimes for KO^{t}Bu + H$_2$O growth. The purple line represents 3 s pulse and 3 s purge. The blue line represents 6 s puls eand 3 s purge. The red line represents 3 s pulse and 6 s purge. The purge after KO^{t}Bu has a separate color for clarity.
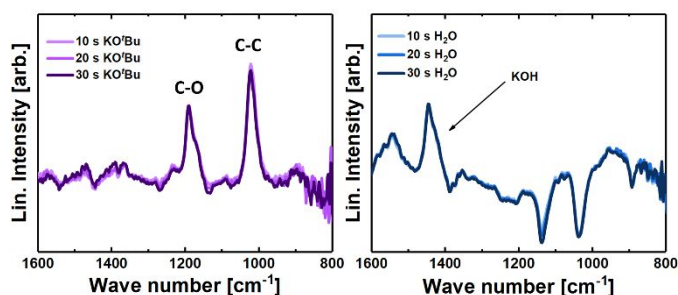
Figure 8: Result of subsequent cycles of KO^{t}Bu + H$_2$O as measured by FT-IR (difference spectra).

Combining the Two – The case of KNbO$_3$

To better understand the effect of using KO^{t}Bu for ternary KNbO$_3$ growth, we revisited the effect of the pulsed ratio between KO^{t}Bu and Nb(OEt)$_5$, and its relationship to GPC and film composition. The inaugural study on this system was carried out in a different reactor tool than what is used here, and as we will see, minor details can have profound effects on the growth.[16] In this study, we find that the K-incorporation and increase in GPC is slightly faster than previously reported. Nonetheless, the same general trends are observed: Rapid K-incorporation even for small pulsed ratios of KO^{t}Bu, and uncontrolled growth as the incorporated level of K goes beyond 50 % (Figure 9). At 1:1 pulsing ratio, the films have large gradients, and visibly react with air upon breaking vacuum, making it hard to stringently analyze them. Stoichiometric KNbO$_3$ is found at 25 cat. % pulsing of KO^{t}Bu. We employed QCM in three different pulsing regimes to emphasize differences in growth depending on the amount of incorporated K. QCM response for a representative supercycle for 3:1 (Nb(OEt)$_5$:KO^{t}Bu) is presented in Figure 10. This is the pulsed ratio that has been shown to result in close to stoichiometric KNbO$_3$. There are several things to notice. The absolute mass gain after KO^{t}Bu and purge is slightly lower than found for "pure" KOH growth, and the mass drop upon the water pulse is slightly less pronounced. This could indicate a lower concentration of KO^{t}Bu adsorbed on the surface. Furthermore, we see that the nature of the Nb(OEt)$_5$ pulses is completely different than for growth of pure Nb$_2$O$_5$. The mass gain upon pulsing Nb(OEt)$_5$ is far lower (~5 vs. 21 ng cyc^{-1}), and the water uptake in the succeeding water pulse is much larger. This is probably a result of the hygroscopic nature of the deposited K-species. However, most of this water is released during subsequent purging. The average mass gain for a full Nb(OEt)$_5$ + H$_2$O cycle for this pulsed ratio, is found to be 7.7 ng cyc^{-1}, approximately half of what was found for pure Nb$_2$O$_5$ growth.
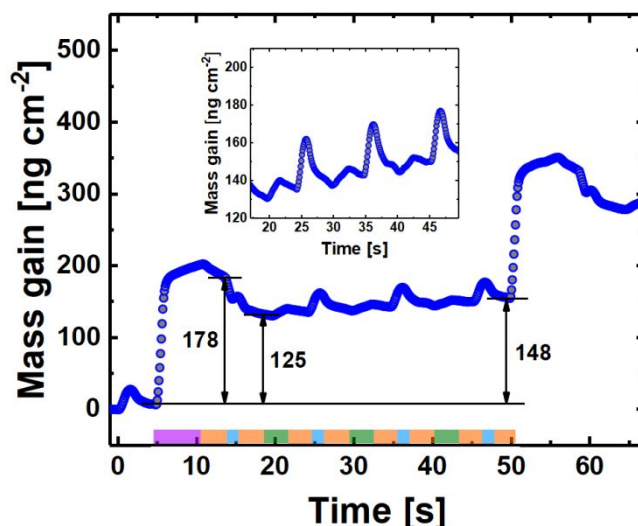
Figure 10: One representative supercycle of 3:1 pulsing (Nb(OEt)5 + H2O:KOtBu + H2O) as measured by QCM. Colored fields indicate KOtBu pulse (purple), purge (orange), water pulse (blue) and Nb(OEt)5 pulse (green), respectively. The inset shows a zoomed in version of the response for Nb(OEt)5 + H2O.

The total mass gain after 3 x [Nb(OEt)$_5$ + H$_2$O] for this pulsing regime is found to be 23 ng cyc^{-1}. Comparing this to the mass gain after KO^{t}Bu + H$_2$O, which is 125 ng cyc^{-1}, we encounter a somewhat mysterious behavior. We know that the 3:1 (Nb(OEt)$_5$:KO^{t}Bu) pulsed ratio facilitates films with total composition close to KNbO$_3$. QCM indicates, however, that much more mass is deposited during KOH growth. In fact, taking the differences in atomic masses into account, there should be *ten* times more K than Nb in the films.

The only plausible explanation for this is that some potassium leaves the surface during the Nb(OEt)$_5$ pulse. Without including this, our estimates above would lead to a strong underestimate of the mass gain of Nb during the Nb(OEt)$_5$ pulse, while at the same time overestimating the total K-incorporation. An interesting feature to support this hypothesis is the initial mass drop we observe during the Nb(OEt)$_5$ pulse (Figure 11). Knowing that potassium *eth*oxide is a relatively stable compound, it is quite possible that K from the large amount of deposited KOH could react with the ethoxide ligands from Nb(OEt)$_5$ in a substitution type reaction, and leave the surface as volatile KOEt. Elucidating this in a more stringent fashion would require surface spectroscopy with higher time resolution than what is available with current technology.

We then turn to more dilute pulsing of KO^{t}Bu, by investigating a representative supercycle for 5:1 (Nb(OEt)$_5$:KO^{t}Bu) by QCM (Figure 12). We find a very similar trend as for 3:1, however with a few notable differences. The mass drop upon water pulsing is slightly higher, leading to less total incorporated K.
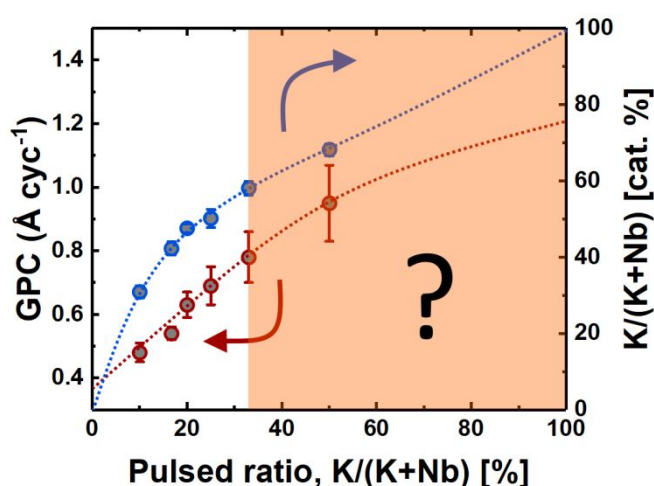

Figure 9: Growth per cycle (left axis, red line) and deposited film cation ratio (K/(K+Nb), right axis blue line) as a function of the pulsed cation precursor ratio (KO^{t}Bu/(KO^{t}Bu + Nb(OEt)$_5$)). Error bars show variation in growth at different places in the reactor.

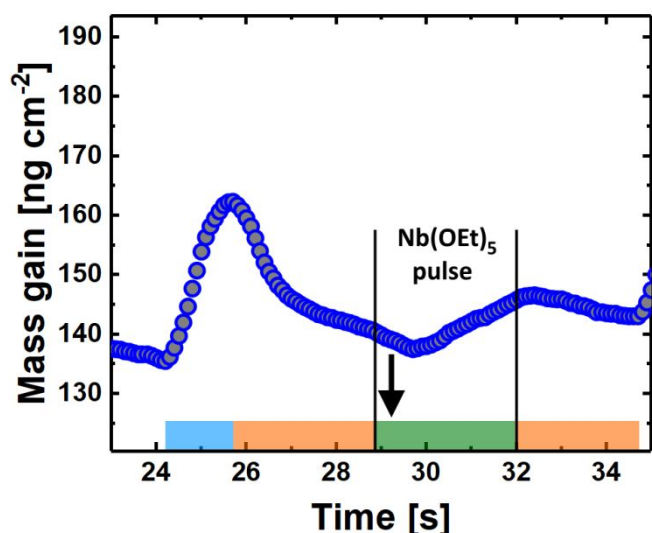Figure 11: One representative Nb(OEt)$_5$ pulse in the 3:1 (Nb(OEt)$_5$ + H$_2$O:KO^{t}Bu + H$_2$O) pulsing regime. Colored fields indicate water pulse (blue), purge (orange) and Nb(OEt)$_5$ pulse (green), respectively.

Figure 13: One representative supercycle of 1:1 pulsing (Nb(OEt)$_5$ + H$_2$O:KO^{t}Bu + H$_2$O) as measured by QCM. Colored fields indicate KO^{t}Bu pulse (purple), purge (orange), water pulse (blue) and Nb(OEt)$_5$ pulse (green), respectively. The inset shows a zoomed in version of the response for Nb(OEt)$_5$ + H$_2$O.

Furthermore, the average mass gain for Nb(OEt)$_5$ + H$_2$O is 9.2 ng cyc^{-1}, slightly higher than for the 3:1 pulsing regime. *I.e.*, KOH grows slower and Nb$_2$O$_5$ grows faster, shifting the film composition towards more Nb. The net increases, however, are still very large and can again only be described by substitution reactions removing K from the surface.

As a final case, we investigated the 1:1 (Nb(OEt)$_5$:KO^{t}Bu) pulsed ratio by QCM (Figure 13). Keep in mind that this has been shown to lead to severe uncontrolled growth. In this regime, we observe a higher total incorporation of K governed by less mass loss upon water pulsing, in addition to almost zero mass increase after Nb(OEt)$_5$ + H$_2$O (only 3 ng cyc^{-1}).

From compositional analysis this ratio leads to approx 20 % Nb in the films, again underpinning that a substitution must take place.

From the insets of figures 10, 12 and 13, note that the water uptake (and release) after Nb(OEt)$_5$ pulsing varies strongly with the pulsed Nb(OEt)$_5$:KO^{t}Bu ratio. The water uptake during the water pulse is approximately double for 1:1 as compared to 5:1. This once again shows that as the concentration of KOH in the films increases, the hygroscopicity becomes stronger. It still seems like most or all of this water is released upon the subsequent purge.

To understand the slow growth of Nb$_2$O$_5$ after incorporating large amounts of K, we studied 200 subsequent cycles of Nb(OEt)$_5$ + H$_2$O after 20 cycles of 1:1 (Nb(OEt)$_5$:KO^{t}Bu). Figure 14 a shows the difference between the first three cycles, and the last three cycles out of the 200, showing a much larger mass increase for the last three cycles. In other words, it is possible to passivate the bulk KOH, moving towards normal Nb$_2$O$_5$ growth. Do, however, notice the large difference between regular Nb$_2$O$_5$ growth (Figure 3) and the cycles in Figure 14 a. It is quite clear that the film bulk still acts as a water reservoir, absorbing large amounts of water that is released during the succeeding purge. The net mass gain after a Nb(OEt)$_5$ + H$_2$O cycle is nonetheless back to normal values after ~50 cycles, after which linear GPC is observed (Figure 14 b).

Figure 12: One representative supercycle of 5:1 pulsing (Nb(OEt)$_5$ + H$_2$O:KO^{t}Bu + H$_2$O) as measured by QCM. Colored fields indicate KO^{t}Bu pulse (purple), purge (orange), water pulse (blue) and Nb(OEt)$_5$ pulse (green), respectively. The inset shows a zoomed in version of the response for Nb(OEt)$_5$ + H$_2$O.

We also studied several subsequent supercycles in the three different ratio regimes using QCM (Figure 15). This analysis shows that within each ratio regime, linear growth is observed. Note that 200 cycles of Nb$_2$O$_5$ were deposited as passivation in between studying the pulsed ratio regimes to limit the effect of preceding K-Nb-O.
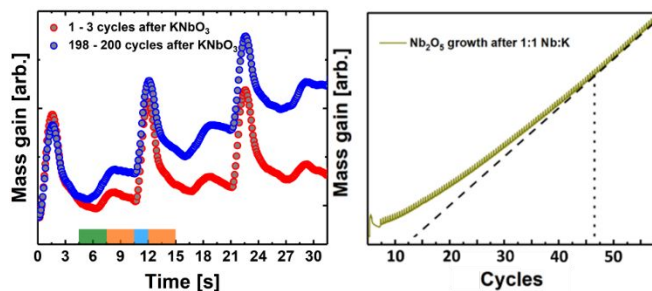
Figure 14: a: Three representative cycles of $Nb(OEt)_5$ + H_2O after deposition of 1:1 $Nb(OEt)_5$ + H_2O:KO^tBu + H_2O. The red line shows the three first cycles after complex deposition, the red line shows cycles 198 – 200 after complex deposition. Colored fields indicate $Nb(OEt)_5$ pulse (green), purge (orange), water pulse (blue) and purge (orange), respectively. Only Nb_2O_5 was deposited in between the red and blue lines. b: The mass gain as a function of the number of cycles after deposition of 1:1 $Nb(OEt)_5$ + H_2O:KO^tBu + H_2O. The dashed line shows a linear extrapolation of the growth after 50 cycles. The dotted line show the number of cycles needed before linear growth is achieved.

Figure 16: Surface functional groups as measured by FT-IR (difference spectra) after the KO^tBu pulse in 1:1 (red), 3:1 (blue) and 4:1 (orange) for $Nb(OEt)_5$ + H_2O:KO^tBu + H_2O.

To finalize the discussion on the effect of pulsing ratio, we carried out *in situ* FT-IR measurements for three different ratio regimes; 1:1, 3:1 and 4:1. Figure 18 shows the state at the surface after the KO^tBu pulse. We clearly observe the stereotypical asymmetric C-O and C-C stretches, with approximately the same surface concentration for all pulsing ratios (slightly lower for 1:1). The major difference, however, is the feature related to KOH at approx. ~1400 cm^{-1}. This feature is not visible for 4:1 and 3:1, but becomes strong for 1:1. This indicates that even without the succeeding water pulse, a large amount of KOH is formed if the concentration of KO^tBu pulses is too high. This can help explain the uncontrollable growth for large K-incorporation, for which KOH is a persisting species that can absorb water and react with air upon breaking vacuum. Finally, we tested an unconventional pulsing regime where the cation precursors are introduced without water pulses. This has been shown to lead to no net growth during deposition, but it can help to shed some light on the substitution that may take place when $Nb(OEt)_5$ reacts with the KOH-terminated surface.
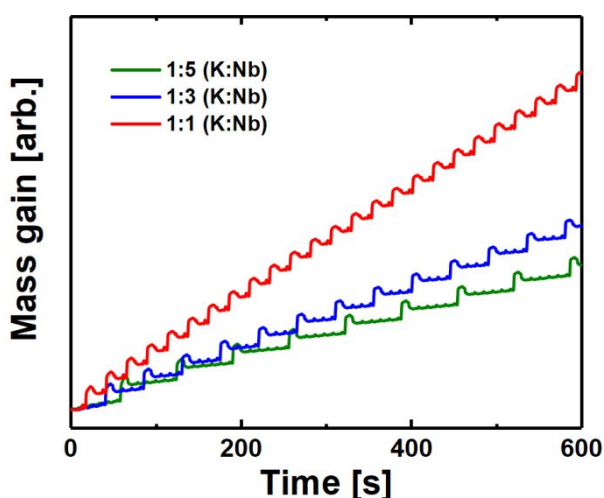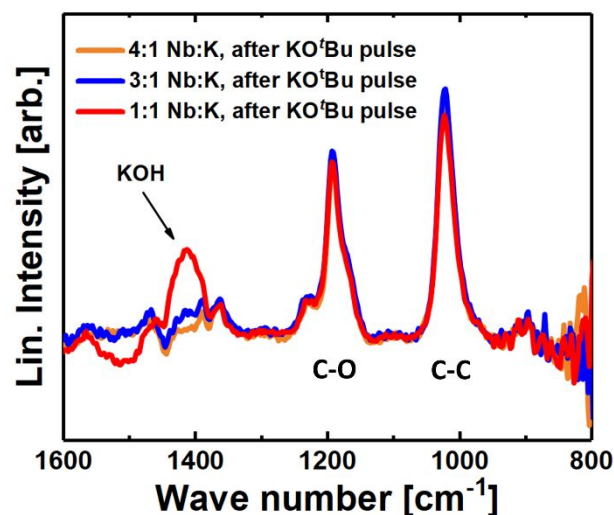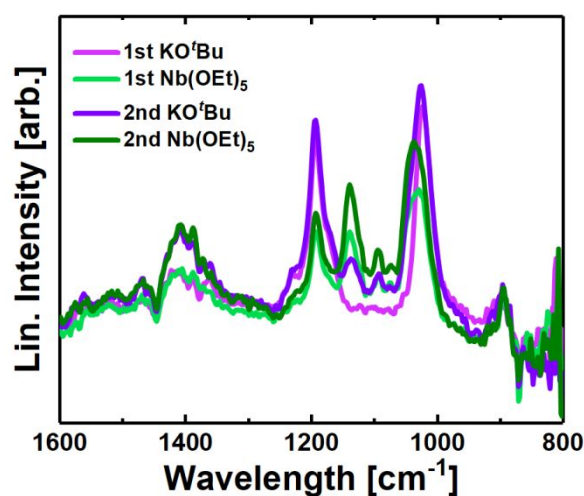
We observe that the first KO^tBu pulse behaves as normal, with clear signals coming from asymmetric C-O stretch with KO^tBu character. Upon pulsing $Nb(OEt)_5$, we clearly see some features from asymmetric C-O-stretches with $Nb(OEt)_5$ character, while some of the KO^tBu character persists. Upon subsequent pulsing of more KO^tBu, this $Nb(OEt)_5$ character is less intense, but still clearly visible, while the KO^tBu character is again enhanced. A second $Nb(OEt)_5$ pulse reenhances the $Nb(OEt)_5$ character, but again some of the KO^tBu character remains. Also note that the signal representing KOH at around ~1400 cm^{-1} is growing for each KO^tBu pulse, but is unchanged after the $Nb(OEt)_5$ pulse. With this behavior, it becomes quite clear that although no net growth is observed, there definitely is a possibility for ligand substitution or some sort of surface rearrangement when combining KO^tBu and $Nb(OEt)_5$. This underpins the complexity of alkali ternary oxide ALD, especially when the cation precursors contain different ligands.

Figure 17: Surface functional groups as measured by FT-IR (difference spectra) for pulsing

Figure 15: Close to linear growth for the three pulsing regimes (1:1 (red), 1:3 (blue) and 1:5 (green)) for $Nb(OEt)_5$ + H_2O:KO^tBu + H_2O

of KO^tBu and $Nb(OEt)_5$. Purple lines denote the FT-IR spectra after the 1st and 2nd KO^tBu, and the green lines denote the FT-IR spectra after the 1st and 2nd $Nb(OEt)_5$ pulses respectively. No water was pulsed in between the cation precursor pulses.

Conclusions

We report on the mechanistic behavior of KO^tBu as a precursor for ALD by stringent *in situ* studies using QCM and FT-IR. The tetrameric nature of KO^tBu has a strong effect on the surface chemistry, and the hygroscopicity of the deposited species affects growth over a large number of cycles. This is shown by evaluating growth of the important complex oxide $KNbO_3$.

We propose that the full KO^tBu tetramer (less a butoxy ligand) is chemisorbed to the surface, which then reacts fast with water upon the water pulse to deposit a large excess of KOH. For large K:Nb-ratios, this leads to uncontrolled water uptake in the subsequent water pulses. We observe that the difference in mass gain upon pulsing of KO^tBu and $Nb(OEt)_5$ is not compatible with the measured film composition. This is most likely countered by a substitution reaction taking place upon pulsing of $Nb(OEt)_5$, in which the niobium precursor reacts with excess KOH on the surface to produce volatile KOEt that is purged out of the reaction chamber. The pulsed ratio between KO^tBu and $Nb(OEt)_5$ impacts the growth on a deeper level, and reactions with water reservoirs in the bulk must be taken into account. This reservoir is largest for high K-concentration.

The behavior of KO^tBu as an ALD precursor is important to be aware of when designing processes for deposition of multi-cation films containing potassium. This includes the technologically important KNN and KTN that are thought to be sustainable replacements for lead-containing materials in piezo-/ferroelectric and electro-optical devices. Furthermore, we believe the behavior of KO^tBu can also help to shed light on Rb- and Cs-containing processes in ALD, for wich the respective *tert*-butoxide share the same tetramer structure.

Conflicts of interest

There are no conflicts to declare.

Acknowledgements

Notes and references

1   E. Østreng, H. H. Sønsteby, T. Sajavaara, O. Nilsen and H. Fjellvåg, *J. Mater. Chem. C.*, 2013, **1**, 4283.
2   R. A. Graham, *Ferroelectrics*, 1976, **10**, 65.
3   X. Meng, D. J. Comstock, T. T. Fister and J. W. Elam, *ACS Nano*, 2014, **8**, 10963.
4   N. Hornsveld, B. Put, W. M. M. Kessels, P. M. Vereecken, M. Creatore, *RSC Adv.*, 2017, **7**, 41359.
5   T. Aaltonen, O. Nilsen, A. Magrasó and H. Fjellvåg, *Chem. Mater.*, 2011, **23**, 4669.
6   E. Østreng, H. H. Sønsteby, S. Øien, O. Nilsen and H. Fjellvåg, *Dalton T.*, 2014, **43**, 16666.
7   H. H. Sønsteby, K. Weibye, J. E. Bratvold and O. Nilsen, *Dalton T.*, 2017, **46**, 16139.
8   M. Zhang, J. S. Yun, Q. Ma, J. Zheng, C. F. J. Lau, X. Deng, J. Kim, D. Kim, J. Seidel, M. A. Green, S. Huang and A. W. Y. Ho-Baillie, *ACS Energy Lett.*, 2017, **2**, 438.
9   T. Duong, Y. Wu, H. Shen, J. Peng, X. Fu, D. Jacobs, E.-C. Wang, T. C. Kho, K. C. Fong, M. Stocks, E. Franklin, A. Blakers, N. Zin, K. McIntosh, W. Li, Y.-B. Cheng, T. P. White, K. Weber and K. Catchpole, *Adv. Energy Mater.*, **7**, 1700228.
10 F. Bella, P. Renzi, C. Cavallo and C. Geribaldi, *Chem. Eur. J.*, 2018, **24**, 12183.
11 J. Liu, M. N. Banis, B. Xiao, Q. Sun, A. Lushington, R. Li, J. Guo, T.-K. Sham and X. Sun, *J. Mater. Chem. A*, 2015, **3**, 24281.
12 Y. Ono, R. Ishikawa, Y. Miyazaki, Y. Ishii, Y. Morii and T. Kajitani, *J. Solid State Chem.*, 2002, **166**, 177.
13 C.-H. Hong, H.-P. Kim, B.-Y. Choi, H.-S. Han, J. S. Son, C. W. Ahn and W. Jo, 2016, *J. Materiomics*, **2**, 1.
14 F. S. Chen, J. E. Geusic, S. K. Kurtz, J. G. Skinner and S. H. Wemple, *J. Appl. Phys.*, 1966, **37**, 388.
15 S. Triebwasser, *Phys. Rev.*, 1959, **114**, 63.
16 H. H. Sønsteby, O. Nilsen and H. Fjellvåg, *J. Vac. Sci. Technol. A*, 2016, **34**, 041508.
17 H. H. Sønsteby, O. Nilsen and H. Fjellvåg, *Global Challenges*, 2019, **3**, 1800114.
18 J. R. Bickford, H. H. Sønsteby, N. A. Strnad, P. Y. Zavalij and R. C. Hoffman, *J. Vac. Sci. Technol. A*, 2019, **37**, 020904.
19 M. H. Chisholm, S. R. Drake, A. A. Naiini and W. E. Streib, *Polyhedron*, 1991, **10**, 337.
20 K. Kukli, M. Ritala, M. Leskelä and R. Lappalainen, *Chem. Vapor Depos.*, 1998, **4**, 29.
21 D. C. Bradley and C. E. Holloway, *J. Chem. Soc. A*, 1968, 219.
22 A. Rahtu, K. Kukli and M. Ritala, *Chem. Mater.*, 2001, **13**, 817.

TOC Entry for "Understanding KOᵗBu in Atomic Layer Deposition - *in situ* Mechanistic Studies of the KNbO₃ Process" – Sønsteby *et al.*
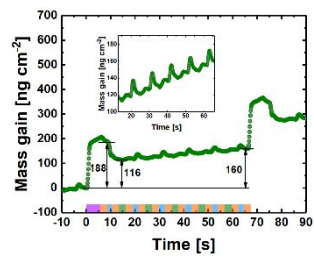
Providing a deeper understanding of alkali metal containing ternary processes by ALD by *in situ* FT-IR and QCM mechanistic studies.